reviews

molecular pharmaceutics

Aqueous Boundary Layers Related to Oral Absorption of a Drug: From Dissolution of a Drug to Carrier Mediated Transport and Intestinal Wall Metabolism

Kiyohiko Sugano*

Global Research & Development, Sandwich Laboratories, Research Formulation, Pfizer Inc., CT13 9NJ, Sandwich, Kent, U.K.

Received April 14, 2010; Revised Manuscript Received July 1, 2010; Accepted July 15, 2010

Abstract: The aqueous boundary layer (ABL) affects various aspects of oral absorption of a drug, from dissolution of the drug to the apparent K_m value of intestinal wall metabolism and carrier mediated transport. However, the importance of ABL has often been entirely ignored in oral absorption investigation. In this minireview, the effect of ABL on oral absorption of a drug is discussed in an easy-to-understand manner. This review starts with an introduction of the boundary layer theory with many illustrations (and links to public web movies visualizing the ABL), and then discusses some specific cases of interest in pharmaceutical science, such as dissolution of floating drug particles in the USP paddle apparatus. The effect of the boundary layer on the membrane permeation is also discussed from the viewpoint of structure permeability relationship, carrier mediated transport/metabolism and estimation of the fraction of a dose absorbed for poor solubility compounds.

Keywords: Dissolution; permeation; mass transfer; Reynolds number; Schmitt number; Sherwood number; laminar; turbulent; oral absorption; aqueous boundary layer; unstirred water layer

1. Introduction

The oral absorption of a drug is affected by several aqueous boundary layers (ABL) which the drug molecules have to pass through to be bioavailable (Figure 1),[1] i.e., ABLs on a drug particle and the intestinal membrane surface which affect the dissolution and permeation rates of the drug, respectively. The purpose of this article is to discuss the ABLs based on the fluid dynamic theory, in a compatible manner to the pharmaceutical sciences. The reason to use the fluid dynamic theory is that it offers insights into the essence of mass transfer and it will improve the experimental design and computational oral absorption simulation in the future. The key equation to translate the fluid dynamics to the pharmaceutical sciences is $Sh/L = 1/h$, where Sh is the Sherwood number, L is the representative length of the object (e.g., the diameter of drug particles and the intestinal tube) and h is the thickness of the ABL in the film model which has been most often used in pharmaceutical sciences. ABL is also referred to as the unstirred water layer (UWL) in pharmaceutical science.

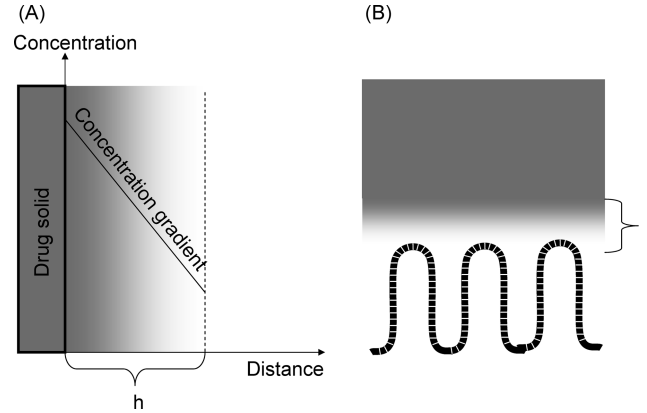

Figure 1. Film model used in the pharmaceutical sciences: (A) dissolution of a drug and (B) intestinal membrane permeation. The gray scale indicates the concentration gradient.

The dissolution and permeation of a drug is called "mass transfer" in this article. Mass transfer of drug molecules by

* Mailing address: Pfizer, Ramsgate Road, Sandwich, Kent, CT13 9NJ, U.K. Tel: +44-1304-644338. Fax: +44-1304-656091. E-mail: Kiyohiko.Sugano@pfizer.com.

(1) Sinko, P. J. *Martin's physical pharmacy and pharmaceutical sciences*; Lippincott Williams & Wilkins: Baltimore, 2006.

10.1021/mp1001119
Published on Web 07/15/2010

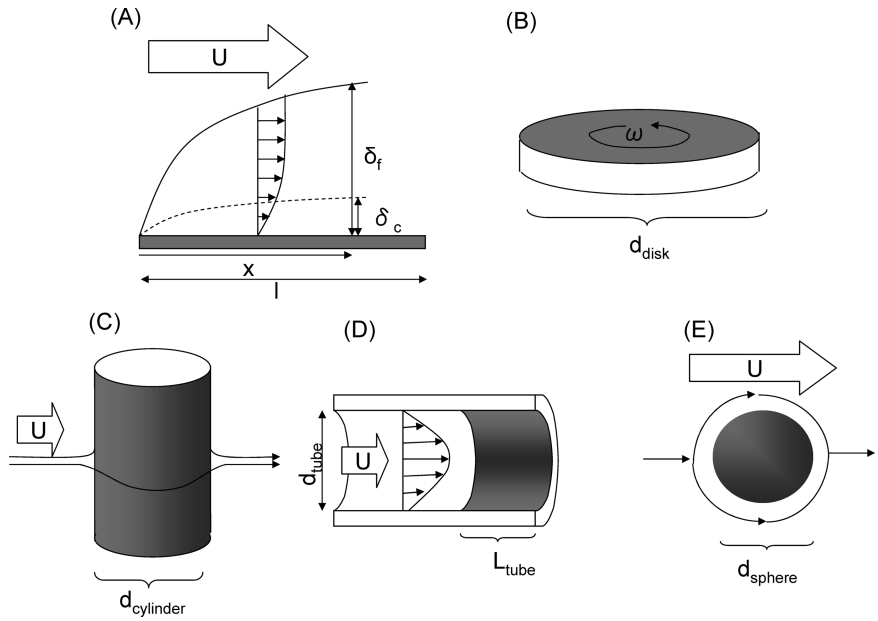

Figure 2. Mass transfer from various objects. The gray part is the surface where mass transfer occurs. (A) A plane in a flow. (B) Rotating disk. (C) Rotating cylinder. (D) Tube flow. (5) A particle in a flow.

convection and diffusion is discussed in the following sections. The first principles of fluid dynamics and mass transfer are mathematically described by the Navier−Stokes and Fick's equations, which are both partial differential equations. In this article, analytical solutions of these equations for the dissolution and permeation of a drug are first discussed using several dimensionless parameters such as the Reynolds number. The application of these analytical solutions for several specific experimental settings used in pharmaceutical science is then discussed. Recent application of computational fluid dynamics (CFD) for pharmaceutical science is also reviewed.

2. Mass Transfer and Sherwood Number

In pharmaceutical science, the dissolution and permeation of a drug is often explained by the film model (Figure 1A).[1] In the film model, the diffusion resistance is represented as the thickness of a diffusion layer (h). The mass transfer rate of a drug can be expressed as

$$\frac{dX}{dt} = SA \cdot D \cdot \frac{1}{h} \cdot \Delta C \tag{1}$$

where SA is the surface area, D is the effective diffusion coefficient, and ΔC is the concentration gradient. This film model is simple and intuitively understandable, hence has been widely used in pharmaceutical science.

In fluid dynamics, the mass transfer from/into an object can be written as

$$\frac{dX}{dt} = SA \cdot k_{mass} \cdot \Delta C = SA \cdot D \cdot \frac{Sh}{L} \cdot \Delta C \tag{2}$$

$$k_{mass} = D \cdot \frac{Sh}{L} \tag{3}$$

where Sh is the Sherwood number and L is the representative length of an object. The representative length is the length of an object in a flow which has the largest influence on the flow around the object of interest. For example, L is defined as the diameter for a particle. Sh characterizes the diffusion resistance of the ABL relative to the representative length (cf. the diffusion resistance has a dimension of length. In pharmaceutical science terms, Sh determines h relative to L).

By comparing eqs 1 and 2, it is trivial that the key to bridge the pharmaceutical sciences and the fluid dynamics is

$$\frac{1}{h} = \frac{Sh}{L} \tag{4}$$

Basically, the local Sherwood number at a point on the object surface could be different point by point (Figure 2A) (in pharmaceutical science terms, h is different point by point). Therefore, to calculate the mass transfer from/to the object, the average of the local Sherwood number for the object is often used. In this article, the Sherwood number means the average Sherwood number of an object unless otherwise indicated.

It should be noted that the effective diffusion coefficient changes in 1 or 2 orders of magnitude depending on the molecular state, e.g., monomer, dimer, micelle bound state (e.g., SDS, bile micelles), cyclodextrin included state, etc. For example, D of bile micelle bound drug molecules is in the $0.1-1 \times 10^{-6}$ cm^2/s range whereas that of free monomer drug molecules is in the $6-10 \times 10^{-6}$ cm^2/s range.[2,3]

(2) Okazaki, A.; Mano, T.; Sugano, K. Theoretical dissolution model of poly-disperse drug particles in biorelevant media. *J. Pharm. Sci.* **2008**, *97* (5), 1843–1852.

(3) Sugano, K.; Okazaki, A.; Sugimoto, S.; Tavornvipas, S.; Omura, A.; Mano, T. Solubility and dissolution profile assessment in drug discovery. *Drug Metab. Pharmacokinet.* **2007**, *22* (4), 225–254.

3. Reynolds and Schmitt Numbers

3.1. Reynolds Number. The Reynolds number (*Re*) is defined as

$$Re = \frac{UL}{\nu} \tag{5}$$

where U is the flow speed around an object and ν is the kinematic viscosity of the fluid. The Reynolds number is often used to characterize the flow of a system, namely "laminar flow" or "turbulence". *Re* is the ratio of inertia of the flow and the viscosity of the fluid. As *Re* increases from single digit to 3−6 digit order, the flow regimen gradually changes from laminar to turbulent. When the viscosity surmounts the inertia, the fluid flow behaves as laminar, whereas when the inertia surmounts the viscosity, the fluid flow behaves as turbulent. The word "turbulence" has gained a lot of popularity and is often used in daily conversation. However, it is important that this word is used correctly when used in the scientific context. The turbulent flow is characterized as the assemblage of fluid dynamical eddies (vortex) of variable scales. Large-scale eddies which could be as large as the flow system (e.g., representative length of the object) are introduced by the contact of the fluid flow to the object. Then the large eddies cascade down to smaller-scale eddies until the energy is dissipated by viscosity. For understanding the essence of turbulence, Lewis Fry Richardson expressed the essence of turbulence as (a parody of On Poetry, A Rhapsody (Swift, 1733)),

> Big whirls have little whirls
> That feed on their velocity
> And little whirls have lesser whirls
> And so on to viscosity
> (in the molecular sense.)
> Lewis Fry Richardson, Weather prediction by numerical process, Cambridge, 1922.

One particular characteristic of turbulent flow is its effective mixing by the eddy diffusion. Basically, straight laminar flow has no mixing effect and only molecular diffusion occurs for spatial spread of molecules, whereas the molecules are carried and spread by the eddies in turbulence (cf. the Reynolds water tube experiments).[4,5] Nowadays, visualization technique had been significantly advanced and many movies are available on the web to understand the flow patterns.[4−7] Several movies of flow visualization are listed in the references, including the Reynolds experiment, to enhance understanding.

3.2. The Concept of Boundary Layer and Schmidt Number. The Navier−Stokes equation is a nonlinear partial differential equation. For most cases of flow patterns and object shapes, it is impossible to derive an exact analytical solution from the NS equation. One approach to solve the NS equation is to apply a physically appropriate approximation(s) to derive approximate analytical solutions, e.g., the boundary layer approximation. Another approach is the computational fluid dynamics in which the Navier−Stokes equation is numerically solved using a high speed computer.

The concept of boundary layer approximation was introduced by Prandtl in 1904. As show in Figrue 2A, on the fluid−object interface, there is a thin fluid layer where the effect of fluid viscosity cannot be neglected. This layer is called "the boundary layer". The existence of a boundary layer on the object surface is directly concluded from the Navier−Stokes equation and no-slip condition at the object surface. In a fluid with viscosity, the boundary layer exists universally on the fluid−solid interface including living substances. For visual understanding, see ref 7. In this boundary layer, as the position in the fluid approaches the object surface, the mass transfer by convection becomes smaller and the molecular diffusion becomes more dominant. At the object surface, there is no flow and the mass transfer is only by molecular diffusion. On the other hand, in the outside of the boundary layer, the mass transfer is dominated by convection. By using this approximation, it becomes easier to obtain an approximate analytical solution for the flows and mass transfer in the boundary layer (the Navier−Stokes equation is converted to the boundary layer equations). This approximation is valid when *Re* is approximately in the range of one to four digits. When *Re* is smaller (called "creeping flow" or "Stokes flow"), the thickness of the boundary layer becomes comparable with the object size and the boundary layer approximation cannot be applicable. In this *Re* range, the Stokes and Oseen approximations can be used to derive analytical solutions from the Navier−Stokes equation. On the other hand, when *Re* is greater than three or four digits, the flow regimen becomes turbulent and the boundary layer approximation is also not applicable.

Figure 2A shows a plane which is put in parallel to a fluid flowing from the left to the right. After the flow senses the head of the plane, the boundary layer starts to grow. At the surface of the plane, there is no flow (no-slip condition). Because of the fluid viscosity, the flow speed near the surface is slower than that of the main flow (U). The concentration boundary layer ($\delta_c(x)$) where a concentration gradient exists is usually much smaller than that of the flow momentum boundary layer ($\delta_f(x)$) in aqueous media (in the following, the variant of position x is omitted). The ratio of the δ_c/δ_f is related to the Schmidt number (*Sc*),

$$\frac{\delta_c}{\delta_f} = Sc^{-1/3} = \left(\frac{\nu}{D}\right)^{-1/3} \tag{6}$$

For example, *Sc* of a typical drug molecule in water is ca. 1000 (MW = 400, $D = 8 \times 10^{-6}$ cm^2/s, $\nu = 0.007$ cm^2/s in water at 37 °C). The boundary layer approximation is valid when $\delta_f \ll L$, $Re > 10-100$ and the flow regimen is laminar. δ_f is usually expressed as

$$\frac{\delta_f}{L} \propto Re^{-1/2} \tag{7}$$

(4) Webpage: Laminar flow in pipe. http://www.youtube.com/watch?v=KqqtOb30jWs&feature=related.
(5) Webpage: Turbulent flow in a pipe http://www.youtube.com/watch?v=NplrDarMDF8&feature=related.
(6) Webpage: Twist in Time - Laminar Flow. http://www.youtube.com/watch?v=p08_KlTKP50.
(7) Webpage: No-Slip Condition. http://www.youtube.com/watch?v=cUTkqZeiMow.

Table 1. Summary of Representative Length, Reynolds Number and Sherwood Number

object[a]	representative length (L)	Reynolds number (Re)	mean Sherwood number (Sh)
plate in a flow (A)	plate length (l_{plate})	$Re_{plate} = \frac{Ul_{plate}}{\nu}$	$Sh_{plate} = 0.66\, Re_{plate}^{1/2}\, Sc^{1/3}$
rotating disk (B)	disk diameter (d_{disk})	$Re_{disk} = \frac{\omega d_{disk}^{2}}{\nu}$	$Sh_{disk} = 0.62\, Re_{disk}^{1/2}\, Sc^{1/3}$
cylinder (C)	cylinder diameter ($d_{cylinder}$)	$Re_{cylinder} = \frac{Ud_{cylinder}}{\nu}$	$Sh_{cylinder} = 0.66\, Re_{cylinder}^{1/2}\, Sc^{1/3}$
tube flow (D)	tube diameter (d_{tube})	$Re_{disk} = \frac{Ud_{tube}}{\nu}$	$Sh_{tube} = 1.52\, Gz^{1/3} = 1.52\left(\frac{d_{tube}}{L_{tube}}\right)^{1/3} \mathrm{Re}_{tube}^{1/3} Sc^{1/3}$
sphere in a flow (E)	sphere diameter ($d_{particle}$)	$Re_{particle} = \frac{Ul_{particle}}{\nu}$	$Sh_{particle} = 2 + 0.6\, Re_{particle}^{1/2}\, Sc^{1/3}$

[a] The letters in parentheses correspond to the panels of Figure 2.

Therefore, when the boundary layer concept is applied, the Sherwood number becomes

$$Sh \propto Re^{1/2}\, Sc^{1/3} \tag{8}$$

These equations (eq 6−8) are valid in a laminar flow. However, even in the turbulent flow, ABL exists (which is called "viscous sublayer").

4. Sherwood Number in Each Flow System

In this section, the relationship among *Sh*, *Re* and *Sc* is discussed. The relating equations are summarized in Table 1. Some of the following equations are a simple approximate analytical solution. More complex analytical solutions to improve the correlation to the experimental data are available in the literature. In addition, CFD has been used to simulate the mass transfer from/into irregular shape objects.[8] However, to keep the perspective straight from eq 8, only the simplest approximate analytical solutions are introduced.

4.1. Planar Surface. In this case, the representative length is the distance from the beginning of the plate ("x" in Figure 2A).[9] The *local* Sherwood number at point "x" is

$$Sh_{plate,local} = 0.33\, Re_{plate,local}^{1/2}\, Sc^{1/3} = 0.33\left(\frac{xU}{\nu}\right)^{1/2}\left(\frac{\nu}{D}\right)^{1/3} \tag{9}$$

$$h = \frac{x}{Sh_{plate,local}} = 3.0x^{1/2}U^{-1/2}\nu^{1/6}D^{1/3} \tag{10}$$

where $Re_{plate,local}$ is the Reynolds number about the distance from the head of the plate,

$$Re_{plate,local} = \frac{Ux}{\nu} \tag{11}$$

Equation 9 is valid in the range of $5 \times 10^2 < Re_x < 5 \times 10^5$. By integrating eq 9, the *mean* Sherwood number for a plate can be

$$Sh_{plate,mean} = \int_0^{l_{plate}} \frac{Sh_{plate,local}}{x}\, dx = 0.66\, Re_{plate}^{1/2}\, Sc^{1/3} = 0.66\left(\frac{l_{plate}U}{\nu}\right)^{1/2}\left(\frac{\nu}{D}\right)^{1/3} \tag{12}$$

where l_{plate} is the length of the plate and used as the representative length. Here, we assume that the solid surface is smooth. In reality, the solid surface cannot be perfectly smooth if observed with a microscope. However, even when the surface of the object is not smooth, if the scale of the irregularity is less than δ_f, the surface is said to be "hydraulically smooth". For example, when the irregularity of a drug particle is in one digit micrometer scale, the surface is hydraulically smooth (cf. section 4.5 and Figure 5).

4.2. Rotating Disk System. In this case, the representative length is the diameter of the disk (d_{disk}) (Figure 2B).[10]

$$Sh_{disk} = 0.62\, Re_{disk}^{1/2}\, Sc^{1/3} = 0.62\left(\frac{\pi \cdot \mathrm{RPM}/60 d_{disk}^{2}}{\nu}\right)^{1/2}\left(\frac{\nu}{D}\right)^{1/3} \tag{13}$$

$$h_{disk} = \frac{d_{disk}}{Sh_{disk}} = 4.98 \cdot \mathrm{RPM}^{-1/2}\nu^{1/6}D^{1/3} \tag{14}$$

where Re_{disk} is the Reynolds number about the rotating disk and RPM is revolutions per minute.

(8) Jia, X.; Williams, R. A. From microstructures of tablets and granules to their dissolution behaviour. *Dissolution Technol.* **2006**, *13* (2), 11–19.

(9) Asano, K. *Basic and application of mass transfer*; Maruzen: Tokyo, 2004.

(10) Polyanin, A. D.; Kutopov, A. M.; Vyazmin, A. V.; Kazenin, D. A. *Hydrodynamics, Mass and Heat Transfer in Chemical Engineering*; CRC Press: New York, 2002.

$$Re_{disk} = \frac{Ud_{disk}}{\nu} = \frac{(\pi d_{disk})\cdot RPM/60 d_{disk}}{\nu} \quad (15)$$

This equation is called the Levich equation. Equation 14 is valid for $10 < Re_{disk} < 10^4$ to 10^5.

4.3. Cylinder System. In this case, the representative length is the diameter of the cylinder ($d_{cylinder}$) (Figure 2C).[9,10] The mean Sherwood number and mean ABL thickness for rotating cylinder are

$$Sh_{cylinder} = 0.66\, Re_{cylinder}^{1/2}\, Sc^{1/3} \quad (16)$$

$$h_{cylinder} = \frac{d_{cylinder}}{Sh_{cylinder}} = \frac{d_{cylinder}}{0.66\left(\frac{Ud_{cylinder}}{\nu}\right)^{1/2}\left(\frac{\nu}{D}\right)^{1/3}} \quad (17)$$

$$Re_{cylinder} = \frac{Ud_{cylinder}}{\nu} \quad (18)$$

4.4. Tube System with a Straight Laminar Flow. The mass transfer in the tube with a straight laminar flow is called "Graetz problem" (Figure 2D). In this case, the representative length is the tube diameter (d_{tube}). However, the mean Sherwood number is also affected by the tube length (l_{tube}).

$$Sh_{tube} = 1.52\, Gz^{1/3} = 1.52\left(\frac{d_{tube}}{l_{tube}}\right)^{1/3} Re_{tube}^{1/3} Sc^{1/3} = 1.52\left(\frac{d_{tube}}{l_{tube}}\right)^{1/3}\left(\frac{Ud_{tube}}{\nu}\right)^{1/3}\left(\frac{\nu}{D}\right)^{1/3} \quad (19)$$

$$h_{tube} = \frac{d_{tube}}{Sh_{tube}} = 0.66\left(\frac{d_{tube} l_{tube} D}{U}\right)^{1/3} \quad (20)$$

$$Re_{disk} = \frac{Ud_{tube}}{\nu}, \qquad Gz = \frac{d_{tube}}{l_{tube}} Re_{tube}\, Sc \quad (21)$$

where Gz is the Graetz number, which is a dimensionless number that characterizes laminar flow in a tube. Equation 19 is called the Leveque equation and is valid at $Gz > 76$. Gz of approximately 1000 or less is the point at which flow would be considered fully developed for mass transfer.

Molecular diffusion through a pore is another interesting topics for pharmaceutical science. The Renkin function is often used as the sieving function.[11] In addition, an electric field function can be added to the Renkin function to incorporate the electrostatic interaction between the diffusing molecule and the pore wall,[12,13] such as in the molecular diffusion through the paracellular pathway of the intestinal epithelial membrane.

4.5. Particles. In this case, the representative length is the diameter of the particle ($d_{particle}$) (Figure 2E). The mean Sherwood number for a spherical particle is represented by the Ranz−Marshall equation as[14]

$$Sh_{particle} = 2 + 0.6\, Re_{particle}^{1/2}\, Sc^{1/3} = 2 + 0.6\left(\frac{Ud_{particle}}{\nu}\right)^{1/2}\left(\frac{\nu}{D}\right)^{1/3} \quad (22)$$

$$h = \frac{d_{particle}}{Sh_{particle}} = \frac{d_{particle}}{2 + \left(\frac{Ud_{particle}}{\nu}\right)^{1/2}\left(\frac{\nu}{D}\right)^{1/3}} \quad (23)$$

$$Re_{particle} = \frac{Ud_{particle}}{\nu} \quad (24)$$

The first term of eq 22 represents the asymptotic diffusion (mass transfer without any flow). The second term represents the contribution of convection. The Ranz−Marshall equation is valid for a wide range of the Reynolds number ($Re_{particle} < 5 \times 10^2$).

The asymptotic diffusion term for a spherical particle (=2 in eq 22) is derived from the concentration gradient around an object induced by spatial expansion (Figure 3A) (detailed derivation of this term is found elsewhere[15,16]). In the case of nonspherical particles, $Sh_{particle}$ deviates from 2. It is convenient to introduce a shape factor (Π) which has a dimension of length as follows.[10]

$$\Pi = Sh_{particle}\frac{SA}{l} \quad (25)$$

In Table 2, equations for several particle shapes are shown. However, in most cases, the particle shape is not exactly the same as listed in the table. For irregularly shaped particles, it is also convenient to use the simple approximation as

$$\Pi = 5.25\, SA^{1/4}\, V^{1/6} \quad (26)$$

where V is the volume of the particle. Figure 4 shows the ratio of the surface area and dissolution rates by asymptotic diffusion for a cylindrical particle having a volume equivalent to a sphere. As the shape of a particle deviates from the sphere, the surface area and dissolution rate increases. However, the extent of increase in the dissolution rate is smaller than that in the surface area. According to eq 26, the dissolution rate remains within 2-fold of the spherical particle of the same volume even when the surface area is

(11) Deen, W. M. Hindered transport of large molecules in liquid-filled pores. *AIChE J.* **1987**, *33* (9), 1409–25.
(12) Adson, A.; Ruab, T. J.; Burton, P. S.; Barsuhn, C. L.; Hilgers, A. R.; Audus, K. L.; Ho, N. F. H. Quantitative approaches to delineate paracellular diffusion in cultured epithelial cell monolayers. *J. Pharm. Sci.* **1994**, *83* (11), 1529–1530.
(13) Sugano, K.; Takata, N.; Machida, M.; Saitoh, K.; Terada, K. Prediction of passive intestinal absorption using bio-mimetic artificial membrane permeation assay and the paracellular pathway model. *Int. J. Pharm.* **2002**, *241* (2), 241–251.
(14) Ranz, W. E.; Marshall, W. R., Jr. Evaporation from drops. I. *Chem. Eng. Prog.* **1952**, *48*, 141–46.
(15) Wang, J.; Flanagan, D. R. General Solution for Diffusion-Controlled Dissolution of Spherical Particles. 1. Theory. *J. Pharm. Sci.* **1999**, *88* (7), 731–738.
(16) Wang, J.; Flanagan, D. R. General solution for diffusion-controlled dissolution of spherical particles. 2. Evaluation of experimental data. *J. Pharm. Sci.* **2002**, *91* (2), 534–542.

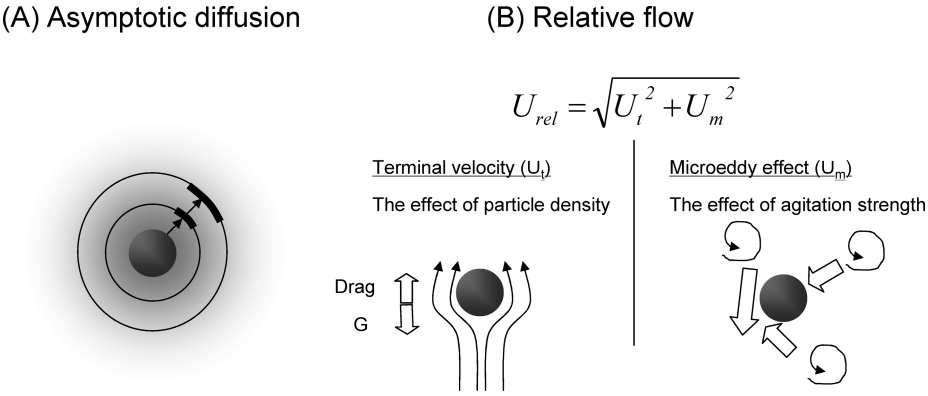

Figure 3. Schematic presentation of particle dissolution. (A) Asymptotic diffusion. The asymptotic diffusion term for a spherical particle is derived from the concentration gradient around an object induced by spatial expansion. The gray scale indicates the concentration gradient. (B) Convection by terminal slip velocity and microeddy effect.

Table 2. Shape Factor for Particles

shape of particle	shape factor $\Pi = Sh(SA)/L$
sphere of diameter d	$2\pi d$
circular cylinder of a diameter d and length L ($0 < L/d < 8$)	$[8 + 4.1(2L/d)^{0.76}]d/2$
cube with edge L	$0.654(2\pi L)$
thin rectangular plate with sides L_1 and L_2 ($L_1 > L_2$)	$2\pi L_1/[ln(4L_1/L_2)]$

increased by 16-fold. In other words, even when the particle shape changes, the ABL on the particle remains a (semi)-sphere and the effectiveness of surface area expansion on the dissolution is masked by this ABL (Figure 5). This theoretical result underwrites the use of volumetric diameter and spherical approximation for small particles where the asymptotic diffusion is dominant.

By the same reason, the surface area measured with the BET technique should be carefully interpreted not to overestimate the dissolution rate of small particles, since the dissolution rate dose not directly reflect the surface area expansion by a serrate surface. Even when the co nvection term in eq 22 is large, the serrate surface of the particle could be hydraulically smooth when irregularity is less than h.

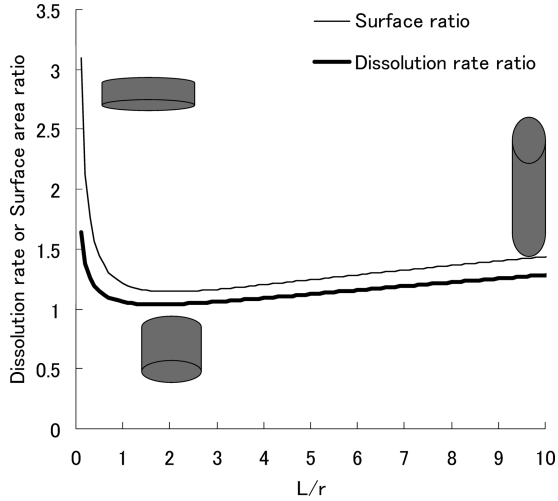

Figure 4. Effect of particle shape on the particle surface and dissolution rate ratios for asymptotic diffusion.

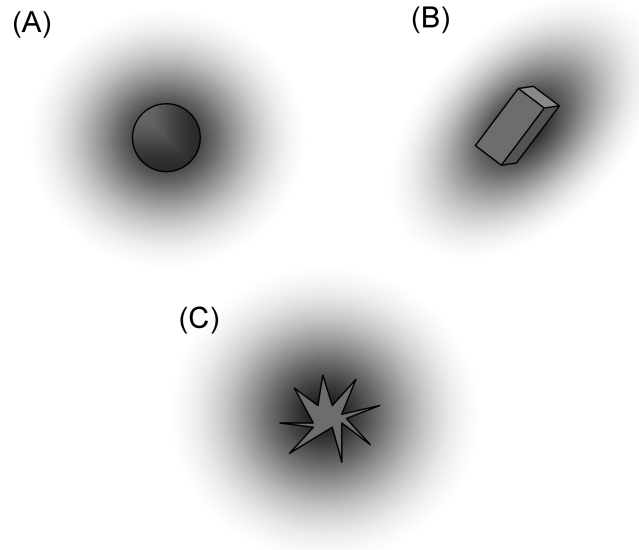

Figure 5. Schematic presentation of concentration gradient by asymptotic diffusion around particles. (A) Sphere. (B) Rectangular. (C) Serrate particle. The gray scale indicates the concentration gradient.

In the case of floating particles, the drug particles move in a synchronic manner with the fluid flow. In this case, Re_{particle} is usually <300, in most cases <1.[17] The relative flow velocity can be approximated to be the sum of terminal velocity (U_t) (Figure 3B) and the microeddy effect which is represented as an expedient fluid velocity induced by the microeddy (U_e).[18−20]

(17) Sugano, K. Theoretical comparison of hydrodynamic diffusion layer models used for dissolution simulation in drug discovery and development. *Int. J. Pharm.* **2008**, *363* (1−2), 73–77.
(18) Armenante, P. M.; Kirwan, D. J. Mass transfer to microparticles in agitated systems. *Chem. Eng. Sci.* **1989**, *44* (12), 2781–96.
(19) Levins, D. M.; Glastonbury, J. F. Particle-liquid hydrodynamics and mass transfer in a stirred vessel. I. Particle-liquid motion. *Trans. Inst. Chem. Eng.* **1972**, *50* (1), 32–41.
(20) Levins, D. M.; Glastonbury, J. R. Particle-liquid hydrodynamics and mass transfer in a stirred vessel. 2. Mass transfer. *Trans. Inst. Chem. Eng.* **1972**, *50* (2), 132–146.

$$U_{rel,tot} = \sqrt{U_t^2 + U_e^2} \quad (27)$$

$$U_t = \frac{(\rho_p - \rho_f) d_{particle}^2 g}{18\mu} \quad (28)$$

$$U_e = 0.195 d_{particle}^{1.1} \varepsilon^{0.525} \mu^{-0.575} \quad (29)$$

where ε is the energy dissipation of turbulence, ρ_f is the fluid density and ρ_p is the particle density. Equation 28 is valid for Stokes flow ($Re < 1$) and should be modified for $Re > 1$ cases.[17] The microeddy effect is related to the turbulence and Kolmogorof's minimum eddy scale (η).[18]

$$\eta = \left(\frac{\upsilon^3}{\varepsilon}\right)^{1/4} \quad (30)$$

For example, η is ca. 100 μm for the USP paddle method with 50 rpm ($\varepsilon = 0.004$ m^2/s^3).[21] A schematic presentation of the microeddy effect is shown in Figure 3B.[22]

When the particle size is small, the particles float in a synchronized manner with the fluid. In this case, the contribution of asymptotic diffusion term becomes dominant as the Reynolds number becomes small and the second term of eq 22 becomes negligible (both U_t and U_e are negligible). For example, small drug particles ($d_{particle} < 60$ μm) floating in the aqueous fluid in the USP paddle method with <100 rpm, asymptotic diffusion becomes dominant and the Sherwood number becomes 2, hence, the thickness of ABL becomes the radius of the particle ($h \approx d_{particle}/2 = r_{particle}$). This is the fluid dynamical explanation for the well-known empirical rule in pharmaceutical sciences that the h is close to the radius of the particles and agitation strength has little effect on the dissolution rate of small particles.[1,23] For coarse particles, the ABL thickness depends on the agitation strength and the density of the particle. As the agitation strength becomes larger, the microeddy effect becomes larger, the ABL thickness then becomes thinner, and the dissolution rate becomes faster. As the true density becomes larger, the terminal sedimentation velocity becomes larger, the ABL thickness then becomes thinner, and the dissolution rate becomes faster.

5. Characterization of Each Dissolution Test Setup Used in Pharmaceutical Science

5.1. Rotating Disk Method. The Levich equation (eq 14) has been used for the rotating disk dissolution test, e.g., the Wood apparatus and μDISS method.[24] The Levich equation theoretically underwrites the experimental finding that the Wood apparatus and μDISS methods gave a similar dissolution rate regardless of the scale of the disk diameter (d_{disk} dose not appear in the Levich equation).[24]

5.2. USP Paddle Method. In the case of the USP paddle method, floating and settled objects should be separately considered.

5.2.1. Floating Particles. In the case of floating particles in a paddle method, the relative flow velocity ($U_{rel,tot}$) can be calculated by eqs 27 − 29, and Sh and h can be then calculated using by eqs 22 − 24. The energy input is different depending on the paddle shape, paddle diameter, etc.

$$\varepsilon = PN \cdot \rho_f N_{paddle}^3 d_{paddle}^5 / Vol \quad (31)$$

where PN is the powder number which is specific to each instrument, N_{paddle} is the rotation speed of the paddle, d_{paddle} is the diameter of the paddle and Vol is the fluid volume. In the case of the USP paddle method with 50 rpm and 1 L fluid volume, ε is 0.004 m^2/s^3.[21] The fluid dynamic model based on the Ranz−Marshall equation has been validated for a wide range of fluid and particle conditions, e.g., agitation strength, fluid and particle densities, etc.[18,20]

Several empirical approximate equations have also been proposed for the dissolution in the USP paddle method. Hintz and Johnson[25,26] proposed an empirical equation (HJ model). The critical h value ($h_{c,HJ}$) was estimated assuming that the h for infinite large particle can be estimated by the Levich equation for a disk method.

$$h = r_p, \qquad r_p < h_{c,HJ} \quad (32)$$

$$h = h_{c,HJ}, \qquad r_p > h_{c,HJ} \quad (33)$$

Wang and Flanagan[15,16] proposed a semiempirical equation based on the film model with a spherical particle (WF model). In their theory, it was hypothesized that the real ABL thickness ($h_{c,WF}$) does not depend on the particle size.

$$\frac{1}{h} = \frac{1}{r_p} + \frac{1}{h_{c,WF}} \quad (34)$$

Figure 6 shows the comparison of HJ, WF, and the fluid dynamic models. $h_{c,HJ}$ and $h_{c,WF}$ are both set to 30 μm, which is most often used in computational oral absorption simulation (in the original paper, $h_{c,WF}$ was reported to be 110 μm).

(21) Crail, D. J.; Tunis, A.; Dansereau, R. Is the use of a 200 mL vessel suitable for dissolution of low dose drug products. *Int. J. Pharm.* **2004**, *269* (1), 203–209.
(22) Houzawa, M.; Toda, M.; Kikuchi, K.-i.; Yonemoto, T.; Tsukada, T. *Diffusion and mass transfer*; Baifu kan: Tokyo, 1996.
(23) Sheng, J. J.; Sirois, P. J.; Dressman, J. B.; Amidon, G. L. Particle diffusional layer thickness in a USP dissolution apparatus II: a combined function of particle size and paddle speed. *J. Pharm. Sci.* **2008**, *97* (11), 4815–4829.
(24) Avdeef, A.; Tsinman, O. Miniaturized Rotating Disk Intrinsic Dissolution Rate Measurement: Effects of Buffer Capacity in Comparisons to Traditional Wood's Apparatus. *Pharm. Res.* **2008**, *25* (11), 2613–2627.
(25) Hintz, R. J.; Johnson, K. C. The effect of particle size distribution on dissolution rate and oral absorption. *Int. J. Pharm.* **1989**, *51* (1), 9–17.
(26) Johnson, K. C. Dissolution and absorption modeling: model expansion to simulate the effects of precipitation, water absorption, longitudinally changing intestinal permeability, and controlled release on drug absorption. *Drug Dev. Ind. Pharm.* **2003**, *29* (8), 833–842.

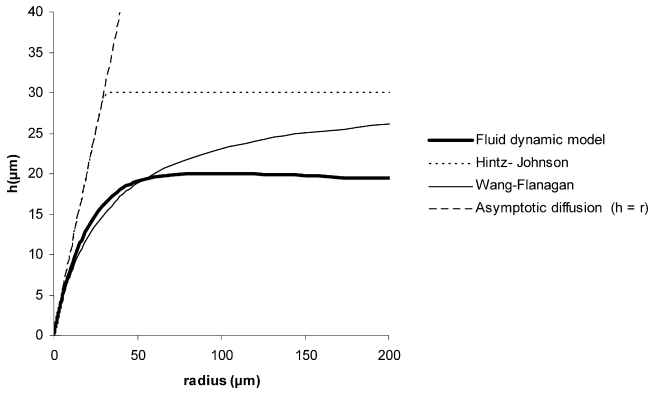

Figure 6. Thickness of ABL estimated by two empirical models (HJ and WF) and the fluid dynamics model. For the fluid dynamic model, drug density and agitation strength were set to 1.2 g/cm^3 and 50 rpm, respectively. $h_{c,HJ} = h_{c,WF} = 30$ μm.

For the HJ model, $h_{c,HJ} = 20$ μm would result in a similar plot with the fluid dynamic model.

The advantages of the fluid dynamic model are that the effects of agitation strength, fluid viscosity and particle density are explicitly taken into account in the equation, and it offers scientifically correct understanding of the mass transfer phenomena. The fluid dynamic model equation is an open analytical solution, so that it does not slow down the computational speed of oral absorption simulation.

When the terminal velocity of particles is larger than an upward flow in a system, the particles would sediment down on the bottom of the system. In this case, the estimation of the Sherwood number would be more complicated, especially when the particles sit close and affect each other's flow pattern.

5.2.2. Tablets on the Bottom. On the other hand, in the case of a settled object such as a tablet on the bottom of the vessel, computational fluid dynamic (CFD) calculation was used to estimate the flow pattern and velocity around the object.[27−31] The absolute flow speed is calculated to be the highest at the edge of the paddle. A spiral upward flow is observed below the paddle. The shear stress is observed around the paddle and vessel wall which would induce large eddies. To estimate the dissolution of a tablet settling on the bottom of the vessel, the U values around the tablet on the bottom of the vessel were calculated by CFD and used with Sh equations to estimate the dissolution rate of the tablet (cf. Figure 2B,C). Similar CFD simulations were also performed for the flow through and other apparatus.[32−35]

6. ABL on Intestinal Membranes

In addition to the dissolution of a drug, ABL can affect the membrane permeation of a drug.

6.1. In Vitro Planar Membranes in a Well Plate (Caco-2, PAMPA, etc.). Since the Levich equation is only valid for mass transfer from a rotating disk, when using a stirring bar placed in parallel to a membrane or orbital shaker, the power above RPM could be different from that of the rotating disk. Therefore, a generalized form of eq 14 was used to fit the experimental mass transfer values.[36,37]

$$h = A' \cdot \mathrm{RPM}^{-B} \cdot D^{1/3} \tag{35}$$

Even when the same RPM is used, the stirring efficacy could be significantly different depending of the configuration of the system. Therefore, A' and B should be obtained for each apparatus.

An orbital shaker is often used for shaking a multiple well plate; however, its agitation efficacy at a moderate speed (e.g., 50−100 rpm) might be poor. A direct stirring method with a stirrer is more effective, such as by using a magnetic stirrer or adding a bead in the well.[37,38] In a 96 well format, when the agitation (stirring) is weak, h becomes 1500−4000 μm.[37]

A subproportional increase of apparent permeability against an increase in agitation strength was sometimes raised as evidence that the dominant permeation barrier has shifted

(27) Bai, G.; Armenante, P. M.; Plank, R. V. Experimental and computational determination of blend time in USP dissolution testing apparatus II. *J. Pharm. Sci.* **2007**, *96* (11), 3072–3086.
(28) Bai, G.; Armenante, P. M.; Plank, R. V.; Gentzler, M.; Ford, K.; Harmon, P. Hydrodynamic investigation of USP dissolution test apparatus II. *J. Pharm. Sci.* **2007**, *96* (9), 2327–2349.
(29) McCarthy Leonard, G.; Bradley, G.; Sexton James, C.; Corrigan Owen, I.; Healy Anne, M. Computational fluid dynamics modeling of the paddle dissolution apparatus: agitation rate, mixing patterns, and fluid velocities. *AAPS PharmSciTech* **2004**, *5* (2), e31.
(30) Bai, G.; Armenante, P. M. Hydrodynamic, mass transfer, and dissolution effects induced by tablet location during dissolution testing. *J. Pharm. Sci.* **2009**, *98* (4), 1511–1531.
(31) Kukura, J.; Arratia, P. E.; Szalai, E. S.; Muzzio, F. J. Engineering tools for understanding the hydrodynamics of dissolution tests. *Drug Dev. Ind. Pharm.* **2003**, *29* (2), 231–239.
(32) Abrahamsson, B.; Pal, A.; Sjoeberg, M.; Carlsson, M.; Laurell, E.; Brasseur, J. G. A Novel in Vitro and Numerical Analysis of Shear-Induced Drug Release from Extended-Release Tablets in the Fed Stomach. *Pharm. Res.* **2005**, *22* (8), 1215–1226.
(33) D'Arcy, D. M.; Corrigan, O. I.; Healy, A. M. Evaluation of hydrodynamics in the basket dissolution apparatus using computational fluid dynamics-Dissolution rate implications. *Eur. J. Pharm. Sci.* **2006**, *27* (2−3), 259–267.
(34) D'Arcy, D. M.; Liu, B.; Bradley, G.; Healy, A. M.; Corrigan, O. I. Hydrodynamic and Species Transfer Simulations in the USP 4 Dissolution Apparatus: Considerations for Dissolution in a Low Velocity Pulsing Flow. *Pharm. Res.* **2010**, *27* (2), 246–258.
(35) D'Arcy, D. M.; Healy, A. M.; Corrigan, O. I. Towards determining appropriate hydrodynamic conditions for in vitro in vivo correlations using computational fluid dynamics. *Eur. J. Pharm. Sci.* **2009**, *37* (3−4), 291–299.
(36) Korjamo, T.; Heikkinen, A. T.; Waltari, P.; Monkkonen, J. The Asymmetry of the Unstirred Water Layer in Permeability Experiments. *Pharm. Res.* **2008**, *25* (7), 1714–1722.
(37) Avdeef, A.; Nielsen, P. E.; Tsinman, O. PAMPA--a drug absorption in vitro model: 11. Matching the in vivo unstirred water layer thickness by individual-well stirring in microtitre plates. *Eur. J. Pharm. Sci.* **2004**, *22* (5), 365–374.
(38) Fujikawa, M.; Nakao, K.; Shimizu, R.; Akamatsu, M. QSAR study on permeability of hydrophobic compounds with artificial membranes. *Bioorg. Med. Chem.* **2007**, *15* (11), 3756–3767.

from the ABL to the membrane. However, as discussed above, h depends on $Re^{-1/2} \sim Re^{-1/3}$. For example, 4-fold increase in the agitation strength would reduce the h only by 1.6−2-fold (cf. eq 35). Therefore, even when permeability becomes less sensitive to the agitation strength, it cannot be simply concluded that the permeation barrier shifted from the ABL to the membrane.

6.2. Intestine under Anesthesia (Rat in Situ Perfusion). The ABL is adjacent to the top of the villi structure (Figure 1). In addition to the fluid viscosity, the mucus layer contributes to maintain the ABL (however, the mucus layer is not a prerequisite of the ABL).

Amidon and co-workers assumed that the intestinal tube is a straight tube with a perfect laminar flow parallel to the tube wall in the rat in situ perfusion study.[39] In this case, the mass transfer across the intestinal tube surface becomes the "Graetz problem" (In their publications, the definition of Gz (Gz') is different from the usual definition [$Gz' = (1/2)Gz^{-1}$]).[9] In a typical experimental condition for a rat intestinal perfusion study (flow speed = 0.2 mL/min, d_{tube} = 0.4 cm, L_{tube} = 10 cm), h was calculated to be ca. 700 μm by eq 19. This is in good agreement with the experimental value of 600−800 μm obtained by using an ABL limited permeation marker drugs.[40] Even though the surface of the intestinal tube is covered by villi, the surface would be hydraulically smooth (Figure 1B). It should be noted that this h value is much thicker than that for nonanesthesia condition.[41]

6.3. Intestine in the Conscious State. The diffusion resistance of the ABL in conscious humans was estimated to be 30−100 μm based on the smooth tube surface.[42,43] When corrected for the fold (plicate) structure (3-fold), the actual thickness of the ABL would be 90−300 μm. This is in good agreement with the mucus layer thickness of 100−200 μm on the villi tip obtained by a direct measurement.[44]

This thin ABL in the conscious humans suggested that the intestinal fluid is effectively agitated, since h is theoretically estimated to be >1 cm by eq 19 based on a straight laminar flow in a tube. This discrepancy between the experimental and theoretical h values suggested that the flow regimen is not a straight laminar flow. At the same time, the Reynolds number calculated for the intestinal tube, tablet and drug particles suggest that the flow regimen around these objects in the intestine could be only weakly turbulent.[45] "Periodical laminar mixing" was suggested to be an additional mechanism for the effective mixing in the gastrointestinal tract.[45]

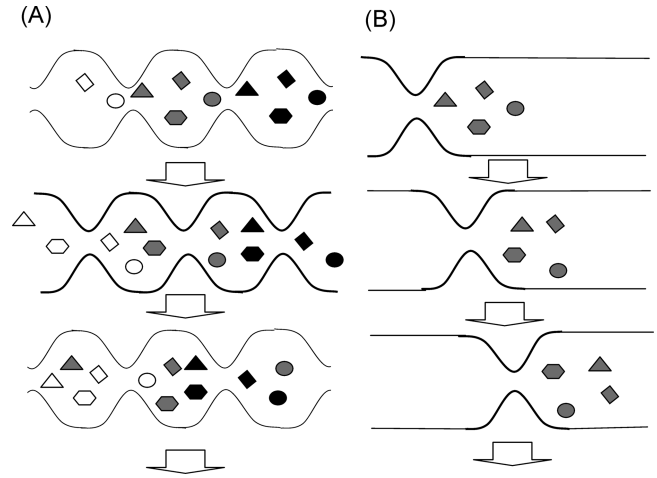

Figure 7. Schematic presentation of segmental contraction (A) and peristaltic movement (B). The arrows indicate the time progression.

There are two types of large scale intestinal wall movement in a conscious state, the periodical segmental contraction and the periodical peristaltic movement; the former was suggested to be the main contributor for mixing whereas the latter moves the chyme toward the distal position (Figure 7). The periodical laminar mixing is also called Baker's transformation (Figure 8). The periodical segmental contraction and peristaltic movement of the intestine would knead and mix the intestinal fluid effectively in spite of the low Re in the intestine with little turbulent flow (= little eddy diffusion and dissipation). In other words, the fluid mixing pattern can be chaotic even without turbulence (periodical laminar mixing is also called "chaotic mixing").[46] This mixing pattern brings the drug and nutrition molecules close to the intestinal wall, hence reduces the ABL thickness. Theoretical estimation of the effect of laminar mixing on the ABL thickness would be the subject for future investigation.

The villous mobility (mainly vertical shrinking),[47,48] which is present in humans and dogs but not in rats, was suggested to be not effective to reduce the ABL thickness.[49] This is in good agreement with the Reynolds number of villi being $\ll 1$ (much smaller than the Re for the intestinal tube scale) and the microfluidics induced by the villous motility is laminar

(39) Kou, J. H.; Fleisher, D.; Amidon, G. L. Calculation of the aqueous diffusion layer resistance for absorption in a tube: application to intestinal membrane permeability determination. *Pharm. Res.* **1991**, *8* (3), 298–305.
(40) Chiou, W. L. Effect of 'unstirred' water layer in the intestine on the rate and extent of absorption after oral administration. *Biopharm. Drug Dispos.* **1994**, *15* (8), 709–717.
(41) Pappenheimer, J. R. Scaling of dimensions of small intestines in non-ruminant eutherian mammals and its significance for absorptive mechanisms. *Comp. Biochem. Physiol., Part A: Mol. Integr. Physiol.* **1998**, *121* (1), 45–58.
(42) Levitt, M. D.; Furne, J. K.; Strocchi, A.; Anderson, B. W.; Levitt, D. G. Physiological measurements of luminal stirring in the dog and human small bowel. *J. Clin. Invest.* **1990**, *86* (5), 1540–1547.
(43) Lennernäs, H. Intestinal permeability and its relevance for absorption and elimination. *Xenobiotica* **2007**, *37* (10/11), 1015–1051.
(44) Atuma, C.; Strugala, V.; Allen, A.; Holm, L. The adherent gastrointestinal mucus gel layer: thickness and physical state in vivo. *Am. J. Physiol.* **2001**, *280* (5, Part 1), G922–G929.
(45) Lentle, R. G.; Janssen, P. W. M. Physical characteristics of digesta and their influence on flow and mixing in the mammalian intestine: a review. *J. Comp. Physiol., B* **2008**, *178* (6), 673–90.
(46) Funakoshi, M. Chaotic mixing and mixing efficiency in a short time. *Fluid Dyn. Res.* **2008**, *40*, 1–33.

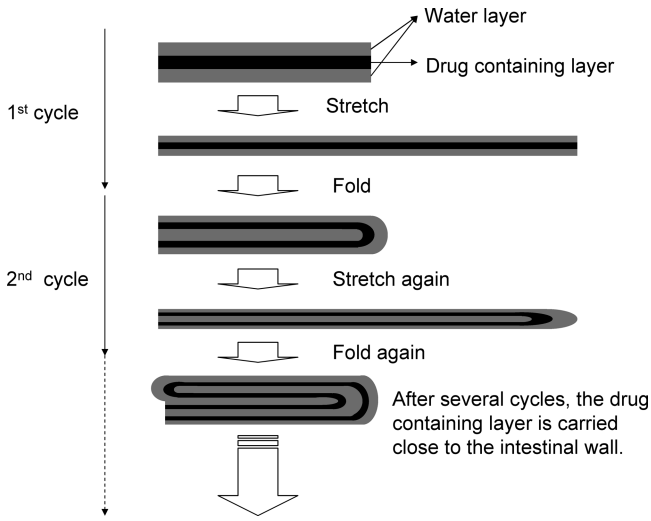

Figure 8. Schematic presentation of Baker's transformation. Even when the flow pattern is perfect laminar, the fluid can be spatially mixed. The mixing pattern presented here is different from the real mixing patter in the intestine, but conveys the essential concept how the laminar mixing occurs and reduces the *h*.

and no mixing would occur.[6] At $Re \ll 1$, viscosity significantly surmounts the inertia of fluid velocity and the fluid is stagnant on the wall, i.e., the villi wall movement. The vertical shrinking movement would not produce a knead and mix pattern.

There were several attempts to experimentally characterize the flow regime of the intestine. Janssen et al. reported that some elements of turbulence were observed when the intestinal fluid had a viscosity close to water, whereas it was absent when the intestinal fluid had higher viscosity such as the fed state chyme.[50]

It should be noted that, when calculating the intestinal membrane permeability in conscious humans using a perfusion technique, Lennernäs and co-workers used the well-mixed model,[43,51] rather than the straight laminar flow tube model which was used for the rat intestinal perfusion study under anesthesia.

7. CFD Simulations for in Vivo Gastrointestinal Tract

The fluid dynamics in the stomach and the pylorus has been investigated using CFD simulation. Pal et al. investigated the role of antral contraction wave (ACW) activity of intragastric fluid motions, pressure and mixing with computer simulation.[52] Gastric mixing was found to be limited to the antrum where occluding ACW generate strong intragastric fluid motions. Dillard et al. investigated the mixing pattern at the pylorus and proximal duodenum. It was found that the asymmetric geometry of the pyloric orifice in concert with intermittent gastric outflow and luminal constriction is likely to enhance homogenization of gastric effluent with duodenal secretion.[53] Since CFD enables us to understand the details of the flow pattern around the formulation in the gastrointestinal tract including inter- and intraindividual variations, it will be a powerful tool for formulation development in the future.

8. Practical Implication of Membrane ABL in Drug Discovery and Development

8.1. Quantitative Structure Permeability Relationship (QSPR). Since the ABL exists ubiquitously adjacent to the membrane, it hinders the measurement of membrane permeability (P_m) when P_m is close or higher than the ABL permeability (P_{ABL}). Therefore, it is necessary to remove the effect of the ABL to obtain an appropriate QSPR.[38] This point has been overlooked in much QSPR literature (i.e., Caco-2 permeability is used regardless of the rate limiting step of apparent permeability).

The apparent permeability (P_{app}) can be expressed as

$$\frac{1}{P_{app}} = \frac{1}{P_{ABL}} + \frac{1}{P_m} = \frac{h}{D} + \frac{1}{P_m} \qquad (36)$$

When $P_{ABL} \ll P_m$, the ABL dominates the total apparent permeability. Increase of agitation strength is often attempted to reduce the ABL thickness.[37,38] When the ABL was removed (experimentally and/or mathematically), the P_{app} value can reach above 0.1 cm/s (i.e., $P_{app} > 100000 \times 10^{-6}$ cm/s).[54] After removal of the ABL and correction for the pH partition theory, a linear free energy relationship can be observed rather than nonlinear relationship. This makes QSPR straightforward.

(47) Womack, W. A.; Barrowman, J. A.; Graham, W. H.; Benoit, J. N.; Kvietys, P. R.; Granger, D. N. Quantitative assessment of villous motility. *Am. J. Physiol.* **1987**, *252* (2, Part 1), G250–G256.
(48) Strocchi, A.; Levitt, M. D. Role of villous surface area in absorption. Science versus religion. *Dig. Dis. Sci.* **1993**, *38* (3), 385–387.
(49) Mailman, D.; Womack, W. A.; Kvietys, P. R.; Granger, D. N. Villous motility and unstirred water layers in canine intestine. *Am. J. Physiol.* **1990**, *258* (2, Part 1), G238–G246.
(50) Janssen, P. W. M.; Lentle, R. G.; Asvarujanon, P.; Chambers, P.; Stafford, K. J.; Hemar, Y. Characterization of flow and mixing regimes within the ileum of the brushtail possum using residence time distributio n analy sis with simultaneous spatio-temporal mapping. *J. Physiol.* **2007**, *582* (Part 3), 1239–1248.
(51) Lennernäs, H. Modeling gastrointestinal drug absorption requires more in vivo biopharmaceutical data: experience from in vivo dissolution and permeability studies in humans. *Curr. Drug Metab.* **2007**, *8* (7), 645–657.
(52) Pal, A.; Indireshkumar, K.; Schwizer, W.; Abrahamsson, B.; Fried, M.; Brasseur James, G. Gastric flow and mixing studied using computer simulation. *Proc. Biol. Sci.* **2004**, *271* (1557), 2587–2594.
(53) Dillard, S.; Krishnan, S.; Udaykumar, H. S. Mechanics of flow and mixing at antroduodenal junction. *World J. Gastroenterol.* **2007**, *13* (9), 1365–1371.
(54) Avdeef, A.; Artursson, P.; Neuhoff, S.; Lazorova, L.; Grasjo, J.; Tavelin, S. Caco-2 permeability of weakly basic drugs predicted with the double-sink PAMPA pKa(flux) method. *Eur. J. Pharm. Sci.* **2005**, *24* (4), 333–349.

In the case of a dissociable compound, the pH−permeability profile is often used to separate P_{ABL} and P_m.[55] According to the pH partition theory, as the portion of undissociated species increases, P_m becomes larger ($1/P_m$ becomes smaller) and P_{ABL} becomes the dominant factor which determines $P_{app.}$ By using this method, h can also be experimentally determined. Since A' and B in eq 35 are specific to an experimental setting, once these values in a system were obtained by using a dissociable compound, it can be used to estimate P_{ABL} for various substrates. P_m can then be calculated using eq 36. It should be noted that the pH−permeability method cannot be directly applied for ex vivo, in situ and in vivo systems since the microclimate pH in the ABL is well maintained.[56,57]

8.2. Carrier Mediated Transport and Metabolism in the Epithelial Cells. Even though the ABL has significant impact on the concentration at the apical membrane surface and in the cytosol,[58,59] the effect of ABL is often overlooked in the carrier mediated transport and metabolic investigations. The concentration of a drug decreases as the position approaches the cell surface. It can be further decreased in the cytosol because of the apical membrane barrier.[60] Therefore, the concentration in the donor compartment should be corrected for the concentration gradient across the ABL−epithelial membrane sequence when intrinsic K_m values from in vitro study such as microsome stability and Pgp ATP-ase assay are used to calculate the intestinal wall metabolism and carrier-mediated transport. In the case when the apical membrane permeability is smaller than ABL permeability, ABL would have little effect on the intestinal wall metabolism and carrier-mediated transport.

8.3. Fraction of a Dose Absorbed (Fa) for Poor Solubility Compounds. The permeability range where ABL has significant impact is $>15-30 \times 10^{-6}$ cm/s (apparent permeability in vitro) and $>1 \times 10^{-4}$ cm/s (effective permeability in humans) which corresponds to >ca. 90% fraction of a dose absorbed (Fa).[61] Therefore, in the case of BCS class III and IV compounds, ABL has little effect on Fa. However, in the case of BCS class II compounds, ABL could have a significant effect on Fa, since the absorbable drug amount in the solubility limited oral absorption case[3,62,63] is determined as the solubility multiplied by permeability.[64,65] For example, even when the two compounds have the same solubility (S) of 0.018 mg/mL, when the in vivo effective permeability (P_{eff}) values are 2 and 8 $\times 10^{-4}$ cm/s, the values of maximum absorbable dose (MAD, eq 37) during the transit time through the small intestine (T_{si}) become 26 mg and 104 mg, respectively.

$$\mathrm{MAD} = 2.3P_{eff}S \times 250\ \mathrm{mL} \times 3.5\ \mathrm{h} \qquad (37)$$

For appropriate estimation of ABL permeability, the apparent in vitro permeability should not be directly used. In a typical experimental setup, the in vitro h value can be significantly different from the in vivo value. In addition, the diffusion coefficient of the bile micelle bound drug molecule is significantly smaller than that of free monomer molecules. A theoretical framework to appropriately treat the difference in ABL thickness and the bile micelle effect has been reported.[66−68] Consideration of ABL was suggested to be the key to understand the food effect,[69] nanoparticle absorption and the dose-dependency of Fa for poor solubility drugs,[70] since the penetration of bile micelle bound drugs

(55) Walter, A.; Gutknecht, J. Monocarboxylic acid permeation through lipid bilayer membranes. *J. Membr. Biol.* **1984**, *77* (3), 255–264.
(56) Hoegerle, M. L.; Winne, D. Drug absorption by the rat jejunum perfused in situ. Dissociation from the pH-partition theory and role of microclimate-pH and unstirred layer. *Naunyn-Schmiedeberg's Arch. Pharmacol.* **1983**, *322* (4), 249–255.
(57) Said, H. M.; Blair, J. A.; Lucas, M. L.; Hilburn, M. E. Intestinal surface acid microclimate in vitro and in vivo in the rat. *J. Lab. Clin. Med.* **1986**, *107*, 420–424.
(58) Korjamo, T.; Heikkinen, A. T.; Moenkkoenen, J. Analysis of unstirred water layer in in vitro permeability experiments. *J. Pharm. Sci.* **2009**, *98* (12), 4469–4479.
(59) Naruhashi, K.; Tamai, I.; Li, Q.; Sai, Y.; Tsuji, A. Experimental demonstration of the unstirred water layer effect on drug transport in caco-2 cells. *J. Pharm. Sci.* **2003**, *92* (7), 1502–1508.
(60) Korjamo, T.; Kemilainen, H.; Heikkinen, A. T.; Monkkonen, J. Decrease in intracellular concentration causes the shift in Km value of efflux pump substrates. *Drug Metab. Dispos.* **2007**, *35* (9), 1574–1579.
(61) Avdeef, A.; Bendels, S.; Di, L.; Faller, B.; Kansy, M.; Sugano, K.; Yamauchi, Y. Parallel artificial membrane permeability assay (PAMPA)-critical factors for better predictions of absorption. *J. Pharm. Sci.* **2007**, *96* (11), 2893–2909.
(62) Yu, L. X. An integrated model for determining causes of poor oral drug absorption. *Pharm. Res.* **1999**, *16* (12), 1883–1887.
(63) Takano, R.; Furumoto, K.; Shiraki, K.; Takata, N.; Hayashi, Y.; Aso, Y.; Yamashita, S. Rate-Limiting Steps of Oral Absorption for Poorly Water-Soluble Drugs in Dogs; Prediction from a Miniscale Dissolution Test and a Physiologically-Based Computer Simulation. *Pharm. Res.* **2008**, *25* (10), 2334–2344.
(64) Dressman, J. B.; Amidon, G. L.; Fleisher, D. Absorption potential: estimating the fraction absorbed for orally administered compounds. *J. Pharm. Sci.* **1985**, *74* (5), 588–589.
(65) Sugano, K. Fraction of dose absorbed calculation: comparison between analytical solution based on one compartment steady state approximation and dynamic seven compartment model. *CBI J.* **2009**, *9*, 75–93.
(66) Amidon, G. E.; Higuchi, W. I.; Ho, N. F. H. Theoretical and experimental studies of transport of micelle-solubilized solutes. *J. Pharm. Sci.* **1982**, *71* (1), 77–84.
(67) Sugano, K. Estimation of effective intestinal membrane permeability considering bile micelle solubilisation. *Int. J. Pharm.* **2009**, *368* (1−2), 116–122.
(68) Sugano, K. Oral absorption simulation for poor solubility compounds. *Chem. Biodiversity* **2009**, *6* (11), 2014–2029.
(69) Sugano, K.; Kataoka, M.; Mathews, C. d. C.; Yamashita, S. Prediction of food effect by bile micelles on oral drug absorption considering free fraction in intestinal fluid. *Eur. J. Pharm. Sci.* **2010**, *40*, 118–124.
(70) Sugano, K. Possible reduction of effective thickness of intestinal unstirred water layer by particle drifting effect. *Int. J. Pharm.* **2010**, *387* (1−2), 103–109.

and small drug particles into the ABL affects the total permeability.

9. Conclusion

This minireview presented a brief introduction of the fluid dynamic concepts into pharmaceutical science. The film model which has been often used in the pharmaceutical sciences is linked to fluid dynamic model equations for mass transfer under a laminar flow via the key equation of $1/h = Sh/L$. The concepts of fluid dynamics may shed light on the future exploration of the sciences of oral absorption of a drug.

Abbreviations Used

D, diffusion coefficient; $d_{cylinder}$, diameter of cylinder; d_{disk}, diameter of disk; d_{paddle}, diameter of paddle; $d_{particle}$, diameter of particle; d_{tube}, diameter of tube; Fa, fraction of dose absorbed; Gz, Graetz number; h, thickness of aqueous boundary layer; $h_{c,HJ}$, critical h value in Hintz−Johnson model; $h_{c,WF}$, critical h value in Wang−Flanagan model; L, representative length of object; l_{plate}, length of plate; l_{tube}, tube length; MAD, maximum absorbable dose; N_{paddle}, rotation speed of paddle; P_{ABL}, aqueous boundary layer permeability; P_{app}, apparent membrane permeability; P_{eff}, in vivo effective permeability; P_m, membrane permeability; PN, power number specific to each instrument; Re, Reynolds number; $Re_{cylinder}$, Reynolds number of cylinder; Re_{disk}, Reynolds number of disk; $Re_{particle}$, Reynolds number of particle; Re_{tube}, Reynolds number of tube; Re_x, Reynolds number about distance from head of plate; $r_{particle}$, radius of particle; RPM, revolutions per minute; S, solubility; SA, surface area of object; Sc, Schmidt number; Sh, Sherwood number; $Sh_{cylinder}$, Sherwood number of cylinder; Sh_{disk}, Sherwood number of disk; $Sh_{particle}$, Sherwood number of particle; Sh_{tube}, Sherwood number of tube; T_{si}, transit time through small intestine; U, flow speed around object; U_e, expedient fluid velocity induced by microeddy; U_{rel}, relative fluid velocity between fluid and particle; U_t, terminal sedimentation velocity; V, volume of particle; Vol, fluid volume of dissolution test; x, distance from head of plate; δ_c, concentration boundary layer thickness; C, concentration gradient; δ_f, flow momentum boundary layer thickness; ε, energy dissipation of turbulence, η, Kolmogorof's minimum eddy scale; μ, kinematic viscosity of fluid; Π, particle shape factor; ρ_f, fluid density; ρ_p, true density of drug particle.

Acknowledgment. K.S. would like to thank Kelly Jones for carefully reading this manuscript.

MP1001119